PHYSICAL REVIEW D **93,** 024014 (2016)

How current loops and solenoids curve spacetime

André Füzfa*

Namur Center for Complex Systems (naXys), University of Namur, Rue de Bruxelles 61, B-5000 Namur, Belgium

(Received 1 April 2015; published 11 January 2016)

The curved spacetime around current loops and solenoids carrying arbitrarily large steady electric currents is obtained from the numerical resolution of the coupled Einstein-Maxwell equations in cylindrical symmetry. The artificial gravitational field associated to the generation of a magnetic field produces gravitational redshift of photons and deviation of light. Null geodesics in the curved spacetime of current loops and solenoids are also presented. We finally propose an experimental setup achievable with current technology of superconducting coils, that produces a phase shift of light of the same order of magnitude as astrophysical signals in ground-based gravitational wave observatories.

DOI: 10.1103/PhysRevD.93.024014

I. INTRODUCTION

Somehow, studying gravity is a contemplative activity: physicists restrict themselves to the study of *natural*, preexisting, sources of gravitation. Generating *artificial gravitational fields*, that could be switched on or off at will, is a question captured or left to science fiction.

However, the equivalence principle, at the very heart of Einstein's general relativity, states that all types of energy produce and undergo gravitation in the same way. The most widespread source of gravitation is the inertial mass, which produces *permanent* gravitational fields. At the opposite, electromagnetic fields could be used to generate *artificial*, or human-made, gravitational fields, that could be switched on or off at will, depending whether their electromagnetic progenitors are present or not.

The equivalence principle actually implies that one also generates gravitational fields when generating electromagnetic fields. However, since the gravitational strength is extremely small compared to the one of the electromagnetic force [1], large electromagnetic fields will only produce tiny spacetime deformations. Yet, electromagnetic fields do curve spacetime. Therefore, general relativity predicts that light and more generally electrically neutral massive particles are deflected by electromagnetic fields, although they do not feel the classical Lorentz force. This effect does not require new exotic physics and it might serve in the future to build new tests of the equivalence principle in the laboratory. In experimental gravity, the permanent gravitational fields involved cannot be withdrawn completely. At the opposite, the gravitational fields generated by electromagnetic fields can be switched off: their experimental search can therefore be done by comparing measurements made in the presence and in the absence of electromagnetic fields. However, due to the weakness of the gravitational interaction, even the strongest magnetic fields humans can currently generate will only produce tiny spacetime deformations. Detecting them would constitute a true experimental challenge which we glimpse at in this paper. Such a detection would nevertheless open the way to new laboratory tests of the equivalence principle.

The so-called Einstein-Maxwell (EM) equations regroup the classical field theories of general relativity and electromagnetism in a covariant way, although without truly unifying them. In some sense, the idea of gravitational field generation from a magnetic field can be attributed to Levi-Cività [2] whose early analytical work describes the curvature of spacetime completely filled by a uniform magnetic field. Subsequent works have established analytical solutions for spacetime around an infinitely long straight wire carrying steady current [3–5]. The main problem of these analytical solutions is that the associated metric is not asymptotically flat, due to the infinitely large current distribution, which makes these analytical solutions of poor interest for practical applications. Overcoming this problem requires considering current distributions of finite extent such as current loops and solenoids. Asymptotic spacetime around current loops carrying steady current has been studied in [5]. An attempt to derive the full solution of EM equations around the current loop was realized a bit later [6]; however this attempt led to an unphysical solution due to an oversimplifying assumption. The case of an infinitely long solenoid was considered in [7] but only for weak perturbations of the metric in linearized general relativity. Therefore, the solutions of the full nonlinear EM equations sourced by the steady currents carried by loops and finite solenoids remained so far unexplored until now.

In this paper, we present two important results: (1) how spacetime is curved around current loops and solenoids carrying *arbitrarily large* electric currents and (2) how the consequent deviation of light could be detected. The structure of this paper is as follows. In Secs. II and III, we develop the numerical resolution of coupled EM equations in cylindrical symmetry. We then present the

*andre.fuzfa@unamur.be

 © 2016 American Physical Society

trajectories of light in curved spacetimes around current loops and solenoids in Sec. IV. In Sec. V, we finally propose an experimental setup based on a modification of interferometers used for the search for gravitational waves and current technology of superconducting electromagnets that produces a detectable artificial spacetime curvature. We conclude by emphasizing the importance of the effect presented here: the deflexion of light in the curved spacetime of an electromagnet opens the way to new experimental tests of Einstein's equivalence principle.

II. EINSTEIN-MAXWELL EQUATIONS FOR THE CURRENT LOOP AND THE SOLENOID

A. Field equations

The EM system models the interaction of gravitation and electromagnetism by their juxtaposition in the following coupled tensorial field equations (in SI units [8]):

$$R_{\mu\nu} = -\frac{8\pi G}{c^4} T^{(\mathrm{em})}_{\mu\nu}, \tag{1}$$

$$\nabla_\mu F^{\mu\nu} = \mu_0 J^\nu \tag{2}$$

where $T^{(\mathrm{em})}_{\mu\nu} = -\frac{1}{\mu_0}(g^{\alpha\beta}F_{\mu\alpha}F_{\nu\beta} - \frac{1}{4}g_{\mu\nu}F_{\alpha\beta}F^{\alpha\beta})$ is the Maxwell stress-energy tensor, $F_{\mu\nu} = \partial_\mu A_\nu - \partial_\nu A_\mu$ is the Faraday tensor of the electromagnetic field, $g_{\mu\nu}$ and A_μ are the metric and the four-vector potential, i.e. the fundamental fields describing gravitation and electromagnetism respectively, $R_{\mu\nu}$ is the Ricci tensor and J^ν the four-current density.

Spacetime is therefore curved by the energy of the electromagnetic field as ruled by Einstein equations of general relativity (1). At the same time, the electromagnetic field propagates in the nontrivial background it generated through Einstein's equations (1), and this propagation is described by the covariant Maxwell equations in curved spacetime (2). Because we are interested in the *additionnal* gravitational field that is produced by the magnetic field, we neglect the mass of the current carriers and the electric wires [9].

Since current loops and solenoids possess one axis of symmetry, we choose the so-called Weyl gauge [5,6,10] for the metric field:

$$ds^2 = c^2 e^{\rho(r,z)}dt^2 - e^{\lambda(r,z)}(dr^2 + dz^2) - e^{-\rho(r,z)}r^2 d\varphi^2. \tag{3}$$

In this symmetry, the vector potential A_μ trivially reduces to one nonvanishing magnetic component $A_\varphi = a(r,z)/r$. The advantage of the Weyl gauge (3) is that the equations of motion directly exhibit usual Laplacian operators on flat background with cylindrical coordinates. Indeed, Eqs. (1) and (2) using Eq. (3) now read (see also [6])

$$\nabla^2_{(r,z)}\rho = \frac{8\pi G}{c^4\mu_0}\frac{e^\rho}{r^2}((\partial_r a)^2 + (\partial_z a)^2), \tag{4}$$

$$\nabla^2_{(r,z)}\lambda + (\partial_z\rho)^2 = \frac{8\pi G}{c^4\mu_0}\frac{e^\rho}{r^2}((\partial_r a)^2 - (\partial_z a)^2), \tag{5}$$

$$\partial_z\lambda + \partial_z\rho = r\partial_r\rho\partial_z\rho + \frac{16\pi G}{c^4\mu_0}\frac{e^\rho}{r}\partial_r a\partial_z a, \tag{6}$$

$$\nabla^2_{(r,z)}a - \frac{2}{r}\partial_r a = -(\partial_r a\partial_r\rho + \partial_z a\partial_z\rho) - r\mu_0 J \tag{7}$$

where $\nabla^2_{(r,z)} = \partial_r^2 + \frac{1}{r}\partial_r + \partial_z^2$ is the usual Laplacian on flat space in cylindrical coordinates and where J is the angular component of the current density. In [6], the term $(\partial_r a\partial_r\rho + \partial_z a\partial_z\rho)$ in Eq. (7) was arbitrarily set to zero to provide an analytical solution. We do not restrict ourselves here to this arbitrary reducing condition and provide the full solution numerically.

Equation (7) is the Maxwell equation on a curved spacetime described by cylindrical coordinates. For a flat Minkowski background $\rho = \lambda = 0$, we have that the nonrelativistic field a_{nr} satisfies

$$\nabla^2_{(r,z)}a_{\mathrm{nr}} - \frac{2}{r}\partial_r a_{\mathrm{nr}} = -r\mu_0 J. \tag{8}$$

We can therefore decompose the total field $a(r,z)$ into the sum of a nonrelativistic part a_{nr} [solution of Eq. (8)] and a relativistic contribution a_{rel} by setting $a = a_{\mathrm{nr}} + a_{\mathrm{rel}}$. The relativistic contribution a_{rel} will therefore be a solution of

$$\nabla^2_{(r,z)}a_{\mathrm{rel}} - \frac{2}{r}\partial_r a_{\mathrm{rel}} = -\{(\partial_r a_{\mathrm{nr}} + \partial_r a_{\mathrm{rel}})\partial_r\rho + \cdots \times (\partial_z a_{\mathrm{nr}} + \partial_z a_{\mathrm{rel}})\partial_z\rho\}. \tag{9}$$

This avoids dealing with pointlike sources representing the current loop and the solenoid in cylindrical coordinates. The source of the field equations now lies in the nonrelativistic contribution $a_{\mathrm{nr}}(r,z)$.

A current loop of radius l corresponds to a current density located on an infinitely thin ring: $J \sim \delta(z)\cdot\delta(r-l)$ while a solenoid of finite length L and of radius l corresponds to a current density located on an infinitely thin sheet located at $r = l$ and $z \in [-\frac{L}{2}, \frac{L}{2}]$ [11]. Analytical expressions of the vector potential A_φ in both cases can be derived from the Biot-Savart law, expressions that of course verify Eq. (8). The nonrelativistic solution $a^{\mathrm{loop}}_{\mathrm{nr}}$ for the current loop is given by [11,12]

$$a^{\mathrm{loop}}_{\mathrm{nr}}(r,z) = \frac{\mu_0 I}{2\pi}\sqrt{(l+r)^2+z^2} \times \left\{\frac{l^2+r^2+z^2}{(l+r)^2+z^2}K(k^2) - E(k^2)\right\} \tag{10}$$

where I is the steady current carried by the wire,

$$k^2 = 4rl((l+r)^2+z^2)^{-1}$$

and

$$K(k^2) = \int_0^{\pi/2} (1-k^2\sin^2(\varphi))^{-1/2} d\varphi,$$
$$E(k^2) = \int_0^{\pi/2} (1-k^2\sin^2(\varphi))^{1/2} d\varphi$$

are the complete elliptic integrals of the first and second kind respectively. For the solenoid of finite length L, the nonrelativistic solution $a_{\rm nr}^{\rm sol}(r,z)$ is given by [13]

$$a_{\rm nr}^{\rm sol}(r,z) = \frac{\mu_0 nI}{4\pi}\sqrt{lr}\times\left[\xi k\left(\frac{k^2+g^2-g^2k^2}{k^2g^2}K(k^2) - \frac{E(k^2)}{k^2}+\frac{g^2-1}{g^2}\Pi(g^2,k^2)\right)\right]_{\xi_-}^{\xi_+} \quad (11)$$

where n is the number of wire loops per unit length,

$$k^2 = \frac{4rl}{((l+r)^2+\xi^2)}, \qquad g^2 = \frac{4rl}{(l+r)^2}, \qquad \xi_\pm = z \pm \frac{L}{2}$$

and

$$\Pi(g^2,k^2) = \int_0^{\pi/2} (1-g^2\sin^2(\varphi))^{-1}(1-k^2\sin^2(\varphi))^{-1/2} d\varphi$$

is the complete elliptic integral of the third kind.

In order to be used as source terms in Eq. (9), the gradients of $a_{\rm nr}(r,z)$ can be obtained analytically from the formulas Eqs. (10) and (11) and the properties of complete elliptic functions.

If we set $r = ul$, $z = vL$ and $a_{\rm nr,rel} \to a_{\rm nr,rel}/(\mu_0 Il)$ [$a_{\rm nr,rel} \to a_{\rm nr,rel}/(\mu_0 nIlL)$ for the solenoid], Eqs. (4), (5), and (9) now reduce to the following set of dimensionless equations

$$\nabla^2\rho = \mathcal{C}_I\frac{L^2}{l^2}\frac{e^\rho}{u^2}\left((\partial_u(a_{\rm nr}+a_{\rm rel}))^2+\frac{l^2}{L^2}(\partial_v(a_{\rm nr}+a_{\rm rel}))^2\right), \quad (12)$$

$$\nabla^2\lambda + \frac{l^2}{L^2}(\partial_v\rho)^2 = \mathcal{C}_I\frac{L^2}{l^2}\frac{e^\rho}{u^2}\left((\partial_u(a_{\rm nr}+a_{\rm rel}))^2 - \frac{l^2}{L^2}(\partial_v(a_{\rm nr}+a_{\rm rel}))^2\right), \quad (13)$$

$$\nabla^2 a_{\rm rel} - \frac{2}{u}\partial_u a_{\rm rel} = -\left(\partial_u(a_{\rm nr}+a_{\rm rel})\partial_u\rho + \frac{l^2}{L^2}\partial_v(a_{\rm nr}+a_{\rm rel})\partial_v\rho\right), \quad (14)$$

$$0 = -\partial_v\lambda + u\partial_u\rho\partial_v\rho - \partial_v\rho + 2\mathcal{C}_I\frac{e^\rho}{u}\partial_u(a_{\rm nr}+a_{\rm rel})\partial_v(a_{\rm nr}+a_{\rm rel}) \quad (15)$$

where $\nabla^2 = \partial_u^2 + \frac{1}{u}\partial_u + \frac{l^2}{L^2}\partial_v^2$. In the following, we will solve Eqs. (12)–(14) numerically and use the last of the Einstein equations Eq. (15) for a validation check.

The dimensionless magnetogravitational coupling for the current loop and the solenoid are given by

$$\mathcal{C}_I^{\rm loop} = \frac{8\pi G}{c^4}\mu_0 I^2; \qquad \mathcal{C}_I^{\rm sol} = \frac{8\pi G}{c^4}\mu_0 I^2 n^2 l^2. \quad (16)$$

Hence it is the square of the total current (I for the loop and InL for the solenoid) that sources the gravitational field [14].

B. Boundary conditions

Solving the system (12)–(14) requires the specification of boundary conditions. On the axis of symmetry, $r = 0$, spacetime must be smooth such that we have $\partial_r\rho|_{r=0} = \partial_r\lambda|_{r=0} = \partial_r a|_{r=0} = 0$. Far away from the current loop or the solenoid [$(u,v) \to (+\infty, \pm\infty)$], these devices behave as magnetic dipoles and the spacetime is asymptotically flat (see also [5]). The magnetic component a is then ruled by Eq. (7) with $\partial_u a\partial_u\rho + \partial_v a\partial_v\rho \approx 0$ (i.e., the nonrelativistic Maxwell equation). This condition is achieved if $a_{\rm rel}$ vanishes and $\partial_v a_{\rm nr} = u\partial_u\psi$ and $\partial_u a_{\rm nr} = -u\partial_v\psi$ with ψ a harmonic function called the scalar magnetic potential [5,6]. For magnetic dipoles, the (dimensionless) scalar magnetic potential is given by

$$\psi = \frac{v}{4}\left(u^2+\frac{L^2}{l^2}v^2\right)^{-3/2}. \quad (17)$$

The metric functions ρ and λ are therefore ruled by the following equations at large distances [$(u,v) \to (+\infty, \pm\infty)$, $\rho \ll 1$ so that $e^\rho \approx 1$]:

$$\nabla^2\rho = \mathcal{C}_I\frac{L^4}{l^4}\left((\partial_u\psi)^2+\frac{l^2}{L^2}(\partial_v\psi)^2\right),$$
$$\nabla^2\lambda = \mathcal{C}_I\frac{L^4}{l^4}\left(\frac{l^2}{L^2}(\partial_v\psi)^2-(\partial_u\psi)^2\right).$$

The asymptotic behaviors for the metric fields around the current loop and the solenoid are therefore given by

$$\rho \sim \frac{\mathcal{C}_{\mathcal{I}}}{32}\frac{L^4}{l^4}v^2\left(u^2+\frac{L^2}{l^2}v^2\right)^{-3}, \quad (18)$$

$$\lambda \sim \frac{\mathcal{C}_{\mathcal{I}}}{16}\frac{L^2}{l^2}\left[2u^2\left(u^2+\frac{L^2}{l^2}v^2\right)^{-3} - \frac{L^2}{l^2}\frac{v^2}{2}\left(u^2+\frac{L^2}{l^2}v^2\right)^{-3} - \frac{9u^4}{4}\left(u^2+\frac{L^2}{l^2}v^2\right)^{-4}\right]. \quad (19)$$

III. NUMERICAL RESOLUTION OF FIELD EQUATIONS

A. Numerical method

We solve Eqs. (12)–(14) numerically by using a combination of relaxation and spectral methods. We first introduce a sequence of functions $\rho^{(n)}(u,v)$, $\lambda^{(n)}(u,v)$ and $a_{\mathrm{rel}}^{(n)}(u,v)$ for the relaxation algorithm such that Eqs. (12)–(14) can be approximated by a set of *linear* inhomogeneous elliptic equations:

$$\nabla^2\rho^{(n+1)} = S_1[\rho^{(n)}, a_{\mathrm{rel}}^{(n)}], \quad (20)$$

$$\nabla^2\lambda^{(n+1)} = S_2[\rho^{(n)}, a_{\mathrm{rel}}^{(n)}], \quad (21)$$

$$\nabla^2 a_{\mathrm{rel}}^{(n+1)} - \frac{2}{u}\partial_u a_{\mathrm{rel}}^{(n+1)} = S_3[\rho^{(n)}, a_{\mathrm{rel}}^{(n)}] \quad (22)$$

where the source terms S_i gather all nonlinear terms of Eqs. (12)–(14) but evaluated with the previous state n of the relaxation algorithm. The algorithm starts with a state $n=0$ that corresponds to the nonrelativistic solution: $\rho^{(0)}(u,v) = \lambda^{(0)}(u,v) = a_{\mathrm{rel}}^{(0)}(u,v) = 0$. At each relaxation step, we solve Eqs. (20)–(22) with a spectral method to compute $\rho^{(n+1)}(u,v)$, $\lambda^{(n+1)}(u,v)$ and $a_{\mathrm{rel}}^{(n+1)}(u,v)$ before iterating. The algorithm is stopped when the relative update of the three fields averaged over the spatial domain reach some tolerance threshold.

To solve Eqs. (20)–(22) at each relaxation step, we develop each field $f(u,v)$ and each source term $S_i(u,v)$ as a truncated Fourier series in the v direction:

$$f(u,v) = \sum_{k=0}^{N}\hat{f}_k(u)\cos\left(\frac{k\pi}{V}v\right); \quad (u,v)\in[0,U]\times[-V,+V]$$

since all the fields are even functions of v due to cylindrical symmetry and where

$$\hat{f}_k(u) = \frac{1}{V}\int_{-V}^{V} f(u,v)\cos\left(\frac{k\pi}{V}v\right)dv.$$

In Fourier space, Eqs. (20)–(22) now become a system of linear inhomogeneous ordinary differential equations (ODEs)

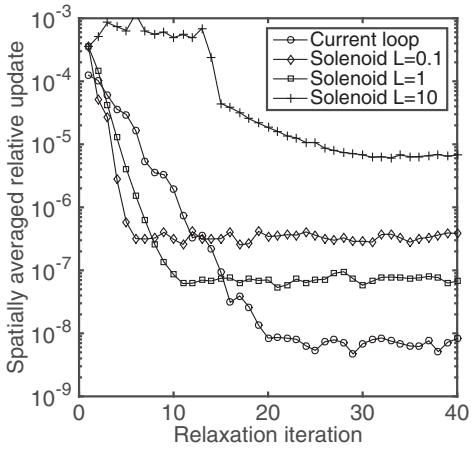

FIG. 1. Relative update on the fields Eq. (26) averaged over the spatial domain, as a function of the relaxation iteration n.

$$\frac{d^2\hat{\rho}_k}{du^2} + \frac{1}{u}\frac{d\hat{\rho}_k}{du} - \frac{l^2}{L^2}\left(\frac{k\pi}{V}\right)^2\hat{\rho}_k = \hat{S}_{k,1}(u), \quad (23)$$

$$\frac{d^2\hat{\lambda}_k}{du^2} + \frac{1}{u}\frac{d\hat{\lambda}_k}{du} - \frac{l^2}{L^2}\left(\frac{k\pi}{V}\right)^2\hat{\lambda}_k = \hat{S}_{k,2}(u), \quad (24)$$

$$\frac{d^2\hat{a_{\mathrm{rel}}}_k}{du^2} - \frac{1}{u}\frac{d\hat{a_{\mathrm{rel}}}_k}{du} - \frac{l^2}{L^2}\left(\frac{k\pi}{V}\right)^2\hat{a_{\mathrm{rel}}}_k = \hat{S}_{k,3}(u) \quad (25)$$

for $k=1,\ldots,N$ and where we have omitted the relaxation index $n+1$. Equations (23)–(25) can be solved as a boundary value problem whose boundary conditions at $u=0$ and $u=U\gg 1$ are the Fourier transforms of the conditions derived in Sec. II B. In the present paper, we have used the algorithm described in [15] for the numerical resolution of Eqs. (23)–(25) for each Fourier mode k at each relaxation step n.

Figure 1 represents the relative update on the fields

$$\frac{1}{3}\left\{\left|\frac{\rho^{(n+1)}}{\rho^{(n)}}-1\right|+\left|\frac{\lambda^{(n+1)}}{\lambda^{(n)}}-1\right|+\left|\frac{a_{\mathrm{rel}}^{(n+1)}}{a_{\mathrm{rel}}^{(n)}}-1\right|\right\} \quad (26)$$

averaged over the spatial domain $[0,U]\times[-V,+V]$, as a function of the relaxation step n. In the relaxation algorithm, the relative updates on the fields decrease exponentially with the number of iterations before settling to some plateau. The algorithm described above therefore converges toward the solution of Eqs. (12)–(14).

We can also have a glimpse of the numerical accuracy of the solution by evaluating the right-hand side of the off-diagonal Einstein equation, Eq. (15), with the fields obtained at the end of the relaxation algorithm. This is illustrated in Fig. 2 in logarithmic scale; the rms of the residual is about 3×10^{-5} for field values of order unity ($\mathcal{C}_I = 1$). The numerical error is more important around the sources of current and are mostly dominated by rounding

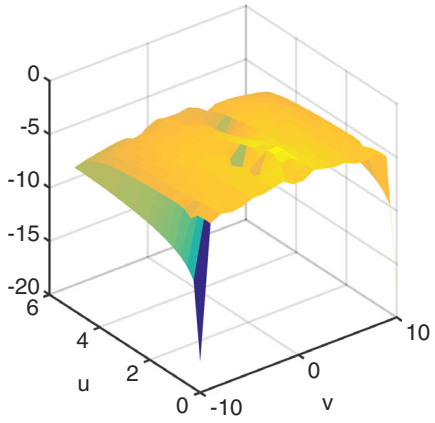

FIG. 2. Right-hand side of Eq. (15) (in logarithmic scale) at the end of the relaxation algorithm (case of a solenoid with $L = 0.1$ and $\mathcal{C}_I = 1$).

errors in the evaluation of the elliptic functions that compose the magnetic potential $a_{\rm nr}$ of the current loop and the solenoid [16].

We can now present the spacetimes curved by the magnetic fields of the current loop and the solenoid.

B. Numerical results

Figures 3 and 4 present the metric functions ρ and λ as well as the relativistic part of the magnetic potential $a_{\rm rel}$ for the current loop (Fig. 3) and solenoids of different lengths (Fig. 4). These plots have been obtained from the numerical resolution of Eqs. (12)–(14) with the boundary conditions Eqs. (18) using the numerical method presented in the previous section.

Metric functions exhibit a peak at the loop location ($u = 1$, $v = 0$) in Fig. 3 and we can notice the similarity between the solutions of the current loops and the solenoid of smaller length (Fig. 4, first row: $L = 0.1$). Spacetime is mostly curved along the radial direction ($v = 0$) inside the loop ($u < 1$) and becomes quickly flat outside of the loop.

When the solenoid length is increased (Fig. 4 from top to bottom), we can see how the metric potential wells deepen and widen along the central z axis. With longer solenoids, the total electric current involved is increased and so is the spacetime deformation at the origin of coordinates. The peak in λ near the solenoid location is also smoothed when the solenoid length is increasing (Fig. 4, central panels from top to bottom). We also have that spacetime deformation occurs mostly inside the solenoid and spacetime becomes quickly flat outside the solenoid.

The total magnetic potential $a = a_{\rm nr} + a_{\rm rel}$ is smaller than in the classical case since we have $a_{\rm rel} < 0$ on average (Figs. 3 and 4, right panels). In general relativity, the electric current produces both magnetic and gravitational fields, leaving less energy to the former than it does in electromagnetism on flat spacetimes. These metric potential wells will produce light deflexion as well as gravitational redshift which will be maximal for a light source located at the origin of coordinates. For an observer located at spatial infinity (where $g_{tt} \to 1$) and a source located at the origin of coordinates, the gravitational redshift is simply $z = 1 - \exp(-\rho(0,0)/2)$, and is of the order of magnitude of the magnetogravitational coupling $\mathcal{C}_I$ (see also Fig. 5). The precision achieved by optical lattice clocks in the measurement of a transition frequency is of the order 10^{-15} [17]. Achieving such a gravitational redshift with single-layered solenoids would require $\mathcal{C}_I \approx 10^{-15}$; i.e. for an electric current of 10^3 A, $n = 100$ it would require a solenoid length of about 10^{11} m. Gravitational redshift therefore does not seem to be appropriate to detect gravitational fields artificially generated by coils with current superconducting technology. As we shall see further, Michelson interferometers with Fabry-Pérot cavities will be more appropriate to attempt such detection of artificially generated gravitational fields.

Figure 5 illustrates how the gravitational redshift z evolves with the magnetogravitational coupling $\mathcal{C}_I$ Eq. (16). For $\mathcal{C}_I \ll 1$, the redshift z varies linearly with $\mathcal{C}_I$ while a spacetime singularity appears at the center of coordinates, $\rho(0,0) \to -\infty$ ($z \to 1$) when $\mathcal{C}_I \to \infty$.

We can now focus on the relativistic effect of the deviation of light by an electric current, through the

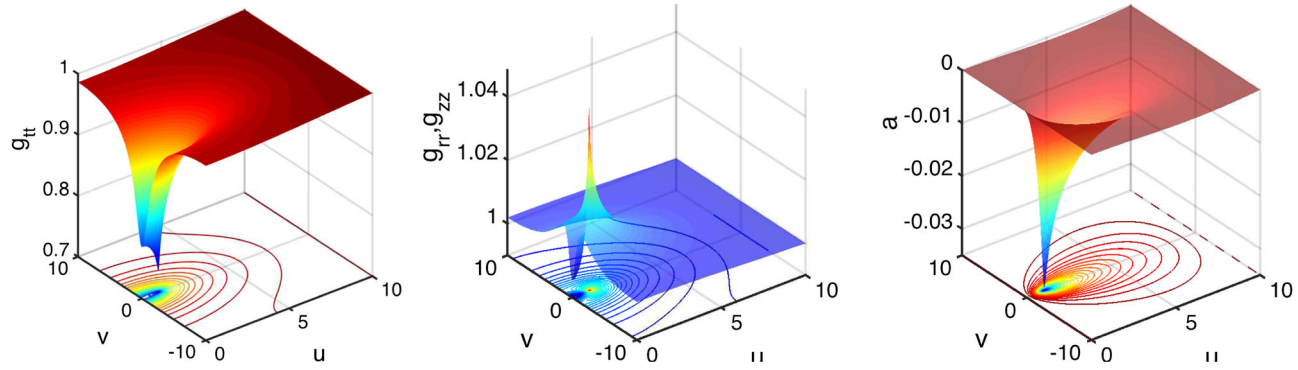

FIG. 3. Metric components and relativistic part of the magnetic potential for the current loop for $\mathcal{C}_I = 1$. Left panel: $g_{tt} = -r^2 g^{\varphi\varphi} = \exp(\rho)$. Central panel: $g_{rr} = g_{zz} = \exp(\lambda)$. Right panel: $a_{\rm rel}$.

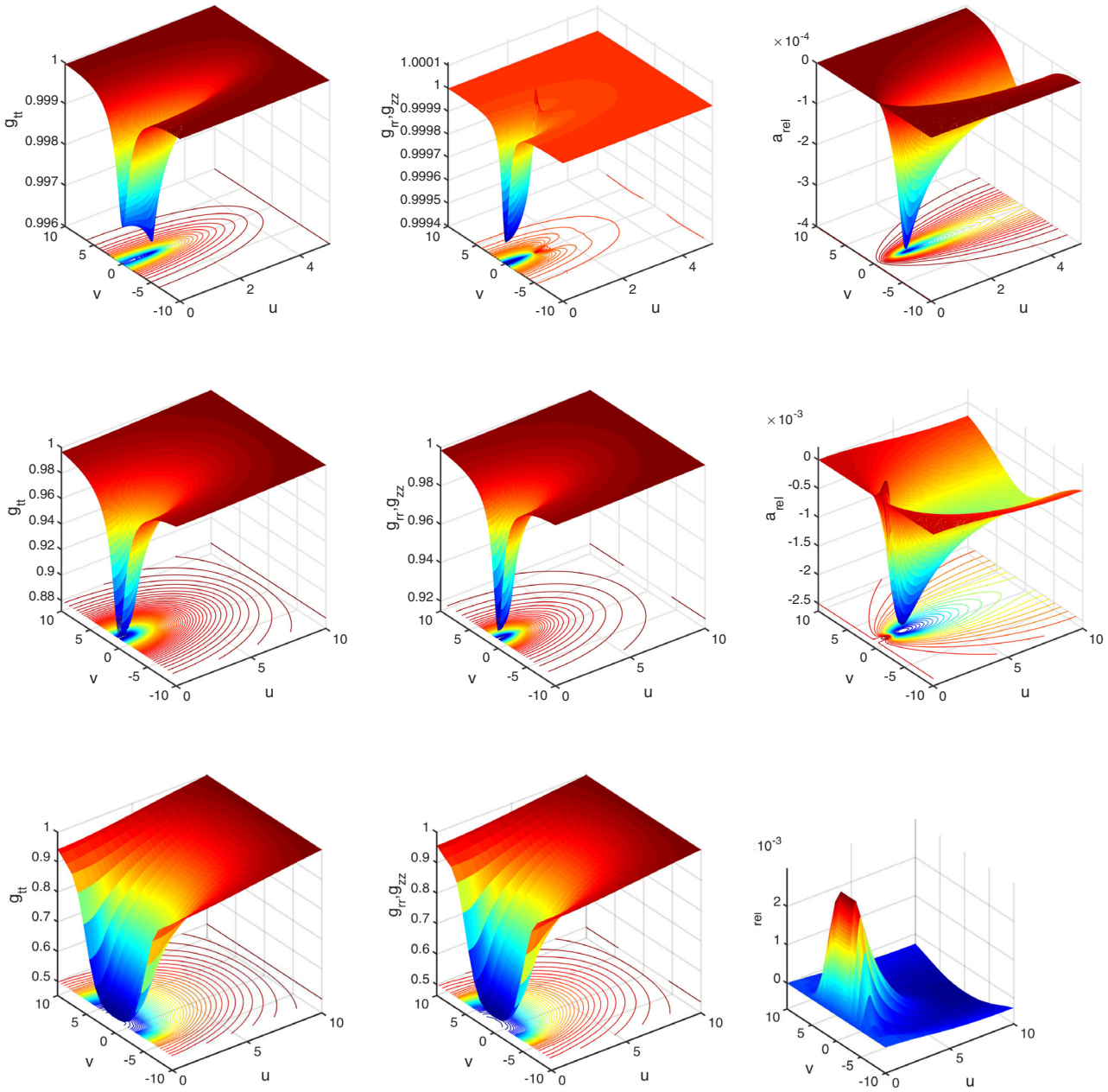

FIG. 4. Metric components and relativistic part of the magnetic potential for solenoids of different lengths for $\mathcal{C}_I = 1$. Left panel: $g_{tt} = -r^2 g^{\varphi\varphi} = \exp(\rho)$. Central panel: $g_{rr} = g_{zz} = \exp(\lambda)$. Right panel: a_{rel}. First row: $L = 0.1$. Second row: $L = 1$. Third row: $L = 10$.

induced deformation of spacetime by magnetic fields. This will be treated in the next section.

IV. THE BENDING OF LIGHT BY MAGNETIC FIELDS IN GENERAL RELATIVITY

In this section, we establish the general pattern of light geodesics in strongly curved spacetimes through numerical integration techniques. The geodesic curves $x^\mu(s)$ of neutral particles are solutions of

$$\frac{d^2x^\alpha}{ds^2} + \Gamma^\alpha_{\beta\gamma}\frac{dx^\beta}{ds}\frac{dx^\gamma}{ds} = 0$$

where s is some affine parameter. Introducing the metric ansatz Eq. (3), this gives the following set of ordinary differential equations:

$$\frac{d^2t}{ds^2} + \frac{\partial\rho}{\partial r}\frac{dt}{ds}\frac{dr}{ds} + \frac{\partial\rho}{\partial z}\frac{dt}{ds}\frac{dz}{ds} = 0, \tag{27}$$

$$\frac{d^2z}{ds^2}+\frac{c^2}{2}e^{\rho-\lambda}\frac{\partial\rho}{\partial z}\left(\frac{dt}{ds}\right)^2+\frac{1}{2}\frac{\partial\lambda}{\partial z}\left(\frac{dz}{ds}\right)^2+\frac{r^2}{2}e^{-\rho-\lambda}\frac{\partial\rho}{\partial z}\left(\frac{d\varphi}{ds}\right)^2+\frac{\partial\lambda}{\partial r}\frac{dz}{ds}\frac{dr}{ds}-\frac{1}{2}\frac{\partial\lambda}{\partial z}\left(\frac{dr}{ds}\right)^2=0, \tag{28}$$

$$\frac{d^2r}{ds^2}+\frac{c^2}{2}e^{\rho-\lambda}\frac{\partial\rho}{\partial r}\left(\frac{dt}{ds}\right)^2-\frac{1}{2}\frac{\partial\lambda}{\partial r}\left(\frac{dz}{ds}\right)^2+\frac{r}{2}e^{-\rho-\lambda}\left(r\frac{\partial\rho}{\partial r}-2\right)\left(\frac{d\varphi}{ds}\right)^2+\frac{\partial\lambda}{\partial z}\frac{dz}{ds}\frac{dr}{ds}+\frac{1}{2}\frac{\partial\lambda}{\partial r}\left(\frac{dr}{ds}\right)^2=0, \tag{29}$$

$$\frac{d^2\varphi}{ds^2}+\left(\frac{2}{r}-\frac{\partial\rho}{\partial r}\right)\frac{dr}{ds}\frac{d\varphi}{ds}-\frac{\partial\rho}{\partial z}\frac{d\varphi}{ds}\frac{dz}{ds}=0. \tag{30}$$

Equations (27) and (30) can be directly integrated to give

$$\frac{dt}{ds}=\frac{1}{c}e^{-\rho}, \tag{31}$$

$$\frac{d\varphi}{ds}=\frac{C}{r^2}e^{\rho} \tag{32}$$

where we chose one integration constant such that the affine parameter s can be identified with the coordinate time ct at spatial infinity (where $\rho\to 0$) and where the constant C is related to the angular momentum of the neutral particle.

For null geodecics, we have that the tangent vector is lightlike all along the geodesic curves $g_{\mu\nu}\frac{dx^\mu}{ds}\frac{dx^\nu}{ds}=0$ so that

$$e^{-\rho}-\frac{C^2}{r^2}e^{\rho}-e^{\lambda}\left[\left(\frac{dz}{ds}\right)^2+\left(\frac{dr}{ds}\right)^2\right]=0. \tag{33}$$

Putting this constraint into the remaining two geodesic equations Eqs. (28) and (29) gives

$$\frac{d^2z}{ds^2}+\frac{C^2}{r^2}e^{\rho-\lambda}\frac{\partial\rho}{\partial z}+\frac{1}{2}\left(\frac{\partial\rho}{\partial z}+\frac{\partial\lambda}{\partial z}\right)\left(\frac{dz}{ds}\right)^2+\frac{1}{2}\left(\frac{\partial\rho}{\partial z}-\frac{\partial\lambda}{\partial z}\right)\left(\frac{dr}{ds}\right)^2+\frac{\partial\lambda}{\partial r}\frac{dz}{ds}\frac{dr}{ds}=0, \tag{34}$$

$$\frac{d^2r}{ds^2}+\frac{C^2}{r^2}e^{\rho-\lambda}\left(\frac{\partial\rho}{\partial r}-\frac{1}{r}\right)+\frac{1}{2}\left(\frac{\partial\rho}{\partial r}-\frac{\partial\lambda}{\partial r}\right)\left(\frac{dz}{ds}\right)^2+\frac{1}{2}\left(\frac{\partial\rho}{\partial r}+\frac{\partial\lambda}{\partial r}\right)\left(\frac{dr}{ds}\right)^2+\frac{\partial\lambda}{\partial z}\frac{dz}{ds}\frac{dr}{ds}=0. \tag{35}$$

In the following, we restrict ourselves to planar trajectories in the (r,z) plane by setting $\varphi=\text{cst}$ and $C=0$ (such that $\frac{d\varphi}{ds}=0$). If we now set $s=Sl$ (and $r=ul$, $z=vL$) we finally obtain the following set of dimensionless ODEs:

$$\frac{d^2v}{dS^2}+\frac{1}{2}\left(\frac{\partial\rho}{\partial v}+\frac{\partial\lambda}{\partial v}\right)\left(\frac{dv}{dS}\right)^2+\frac{l^2}{2L^2}\left(\frac{\partial\rho}{\partial v}-\frac{\partial\lambda}{\partial v}\right)\left(\frac{du}{dS}\right)^2+\frac{\partial\lambda}{\partial u}\frac{dv}{dS}\frac{du}{dS}=0, \tag{36}$$

$$\frac{d^2u}{dS^2}+\frac{L^2}{2l^2}\left(\frac{\partial\rho}{\partial u}-\frac{\partial\lambda}{\partial u}\right)\left(\frac{dv}{dS}\right)^2+\frac{1}{2}\left(\frac{\partial\lambda}{\partial u}+\frac{\partial\rho}{\partial u}\right)\left(\frac{du}{dS}\right)^2+\frac{\partial\lambda}{\partial v}\frac{dv}{dS}\frac{du}{dS}=0. \tag{37}$$

Since the metric fields and their derivatives are all functions of (u,v) coordinates, solving Eqs. (36) and (37) requires integrating both ODEs while carefully interpolating the numerical fields λ, $\partial_{u,z}\lambda$, ρ, $\partial_{u,z}\rho$ at the current location point in each integration step. Equation (33) will be used as a constraint to validate the numerical integration.

Figure 6 presents the deflected trajectories of a bundle of light rays incoming parallel from spatial infinity $v\to+\infty$. These trajectories have been obtained from the numerical resolution of geodesic equations in strongly curved spacetimes around loop and solenoids with extremely large magnetogravitational coupling $\mathcal{C}_I=10$ (or $\mathcal{C}_I=1$) so that the way light is deflected can be easily shown. The constraint Eq. (33) is below 10^{-8} along the trajectories shown in Fig. 6.

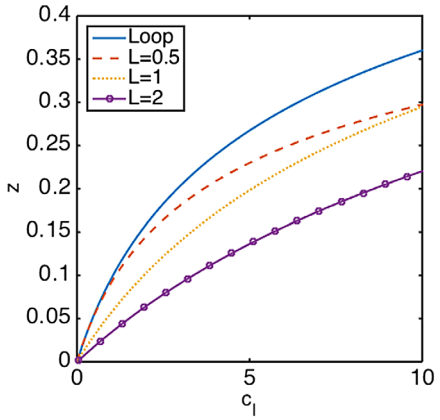

FIG. 5. Gravitational redshift of a light source located at the center of coordinates and a receiver at spatial infinity, as a function of the magnetogravitational coupling $\mathcal{C}_I$.

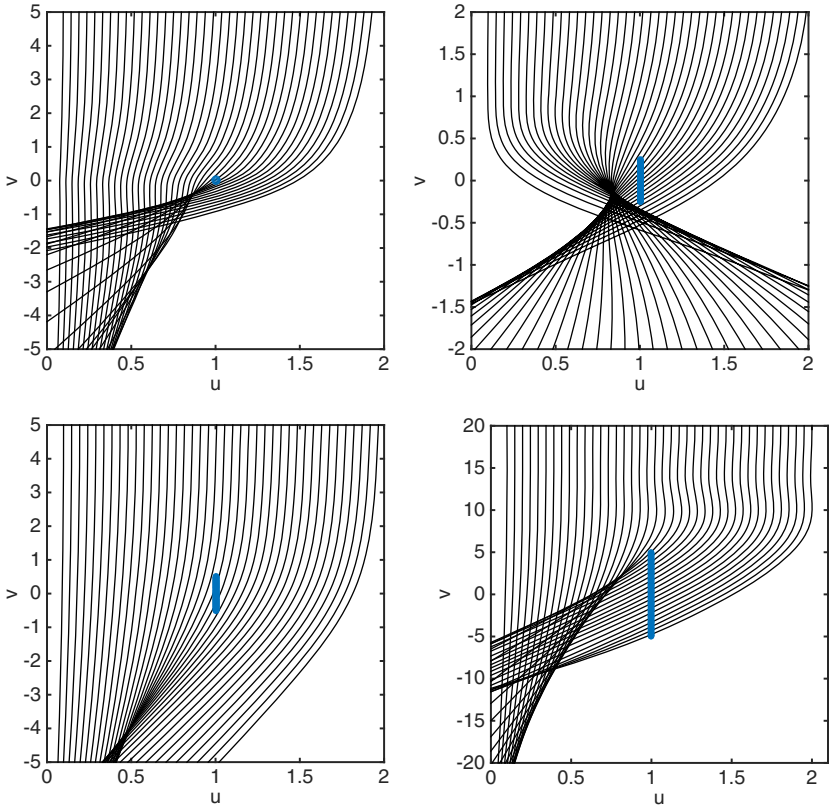

FIG. 6. Trajectories of parallel light rays coming from infinity. Top left panel: current loop ($\mathcal{C}_I = 10$). Top right panel: solenoid with $L = 0.5l$ ($\mathcal{C}_I = 10$). Lower left panel: solenoid with $L = l$ ($\mathcal{C}_I = 10$). Lower right panel: solenoid with $L = 10l$ ($\mathcal{C}_I = 1$). Blue dots indicate the location of the current loop and the solenoids.

Geodesics passing far away from the current loop of the solenoid follow hyperbola as if photons were attracted by a point mass. However, null geodesics with close encounters can exhibit more sophisticated shape while passing through the magnetic device. In this case of strong coupling ($\mathcal{C}_I = 10$ or $\mathcal{C}_I = 1$), the deviation of the light beam is so strong that magnification appears at some locations while large regions of the (u, v) plane have been cleared of any light. These results can be applied to the gravitational lensing of cosmic string loops in the strong field regime.

V. APPLICATION: GENERATION AND DETECTION OF ARTIFICIALLY GENERATED GRAVITATIONAL FIELDS

We now investigate how far such deflexion of light could be detected with the present technology of superconducting electromagnets and high precision light-wave interferometers. The basic idea is to make interfering two light beams among which one has traveled in the spacetime curved by powered superconducting solenoids and the other not. The shorter distances traveled by the light beam inside the powered solenoids will generate a path difference between both light beams that will impact their interference pattern as a result of a gravitationally generated phase shift. However, since the large electric currents that can be achieved with current superconducting cables, roughly of order $10^4 A$, will generate extremely weak spacetime curvature, it will be necessary to amplify the signal by forcing light to perform numerous round-trips in the artificially generated gravitational field.

We can first write down the gravitational field equations in the weak field limit. If we assume $a_{\mathrm{rel}} \ll a_{\mathrm{nr}}$ and ρ, $\lambda \ll 1$, we get that Eqs. (12) and (13) now reduce to

$$\nabla^2\rho = \frac{\mathcal{C}_I}{u^2}\frac{L^2}{l^2}\left((\partial_u a_{\mathrm{nr}})^2 + \frac{l^2}{L^2}(\partial_v a_{\mathrm{nr}})^2\right), \tag{38}$$

$$\nabla^2\lambda = \frac{\mathcal{C}_I}{u^2}\frac{L^2}{l^2}\left((\partial_u a_{\mathrm{nr}})^2 - \frac{l^2}{L^2}(\partial_v a_{\mathrm{nr}})^2\right) \tag{39}$$

where $\nabla^2 = \partial_u^2 + \frac{1}{u}\partial_u + \frac{l^2}{L^2}\partial_v^2$. For reasons to be explained below, we will consider that the source of the magnetic fields is given by a set of stacked anti-Helmholtz coils (or multilayered coils). The ith anti-Helmholtz coil is constituted by two solenoids of radius l_i ($l_i < l$), length L, spaced by a distance D and carrying steady electric current of opposite directions. It will be necessary to pile up these (anti-)Helmholtz coils to produce a detectable spacetime curvature by means of electric currents of order $10^4 A$. The corresponding expression for the total magnetic potential a_{nr} of n stacked anti-Helmholtz coils of radius l_i can be obtained from Eq. (11) by

$$a_{\mathrm{nr}} = \sum_{i=1}^{n}\left(a_{\mathrm{nr}}^{\mathrm{sol}}(r, z + D/2; l_i) - a_{\mathrm{nr}}^{\mathrm{sol}}(r, z - D/2; l_i)\right). \tag{40}$$

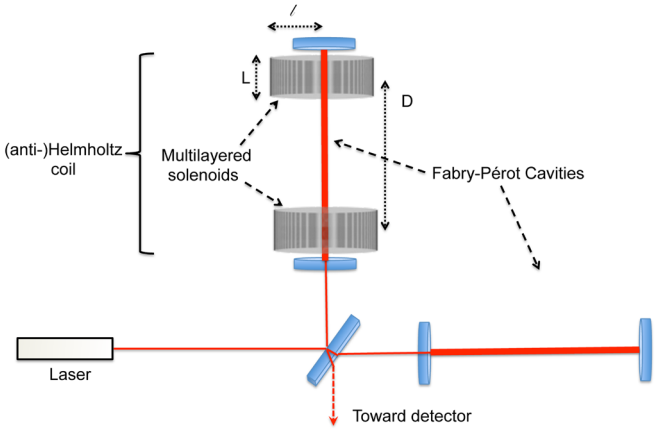

FIG. 7. Schematic view of the proposed experimental setup.

Corresponding boundary conditions can be obtained from those given in Sec. II by linearly superposing the boundary conditions of single solenoids as allowed by the weak gravitational field limit. The problem can be solved numerically with a standard spectral method (for instance based on Fourier decomposition; see Sec. III).

Our proposed experimental setup shown in Fig. 7 recalls those of ground-based interferometers used to detect gravitational waves: it consists of a Michelson interferometer whose arms are constituted by Fabry-Pérot cavities. One of these arms goes through a multilayered anti-Helmholtz coil consisting of two stacks of superconducting solenoids. As long as the electric current is switched on in the device, this one curves spacetime and deflects light. Since spacetime is slightly shrunk inside the coil, light trapped inside the powered coil accumulates phase shift as the round-trips succeed each other.

Following [18], we can write down the phase shift due to the weak gravitational field $h_{\mu\nu}$ on a Minkowski path γ of light

$$\Delta\Phi = \frac{1}{2}\int_{\gamma} h_{\mu\nu}K^{(0)\nu}dx^{\mu} \tag{41}$$

where $K^{(0)\nu}$ is the (unperturbed) constant 4-wave vector of the wave front. We focus on light following the axis $u = 0$ of the coil, with wave vector components $K^{(0)t} = \frac{2\pi\nu}{c} = K^{(0)z}$ with ν the frequency of light. Therefore, the phase shift along the axis of the coil for one trip is given by

$$\Delta\Phi = \frac{\pi}{\Lambda}\int_0^{\mathcal{L}} (\rho(0,z) - \lambda(0,z))dz \tag{42}$$

where $\Lambda = \frac{c}{\nu}$ is the wavelength of the light beam of frequency ν and $\mathcal{L}$ is the length of the interferometer arm. An anti-Helmholtz coil configuration is better than a solenoid for the production of gravitational phase shift. Indeed, phase shift is directly related to the difference $\rho - \lambda$ which obeys the following partial differential equation [Eqs. (38) and (39)]:

$$\nabla^2(\rho - \lambda) = \frac{2\mathcal{C}_I}{u^2}(\partial_v a_{\rm nr})^2 \sim |B_r|^2, \tag{43}$$

where B_r is the radial component of the magnetic field. This quantity, although vanishing on the axis of symmetry, increases more rapidly inside a Helmholtz coil than in the interior of a long solenoid, justifying the above-mentioned choice. As a matter of comparison, the phase shift induced by a gravitational wave passing by a Michelson interferometer is given by [19]

$$\Delta\Phi = \frac{2\pi c}{\Lambda}|h|\tau_{\rm trip} \tag{44}$$

where $|h|$ is the amplitude of the incoming gravitational wave and $\tau_{\rm trip} = 2\mathcal{L}/c$ is the single round-trip travel time of the light beam inside the arm (to be amplified through the multiple reflections induced by the Fabry-Pérot cavities). Currently the achievable threshold for detection is for $|h| \approx 10^{-21}$, $\mathcal{L} \approx 10^3$ m and $\Lambda \approx 10^{-6}$ m yielding $\Delta\Phi \approx 10^{-11}$ rad per trip.

Let us now give an estimation of this phase shift for realistic experimental conditions of the setup presented above. We particularize the setup as follows. We consider a set of ten stacked anti-Helmholtz coils, each constituted by two superconducting solenoids of same length $L = 2.5$ m carrying opposite steady electric current of 2×10^4 A (which is similar to CMS-class magnets [20]) spaced by a distance of $D = 2.5$ m. The external solenoids have a radius of $l = 5$ m and the ten solenoid shells are chosen equally spaced between $r = 1$ m and $r = 5$ m. The length of the interferometer arm has been chosen to $\mathcal{L} = 50$ m.

Figure 8 shows the profiles of $B_z(0,v)$ and $\rho(0,v) - \lambda(0,v)$ along the axis of symmetry $u = 0$ of the solenoids. The anti-Helmholtz coils generate a curvature of spacetime that reaches its maximum at mid-distance from each of the solenoids ($u = 0$, $v = 0$) where the magnetic field vanishes. The magnetic field is maximal at the center of the solenoids (at $z = \pm D/2$), and its magnitude reaches about $20T$ for the parameters chosen above. The phase shift Eq. (42) can be integrated numerically for the results of Fig. 8 and we find $\Delta\phi \approx -1.56 \times 10^{-25}$ (for $\Lambda 514$ nm) per round-trip inside the interferometer. If the experiment can be conducted long enough, for a time $T_{\rm exp}$, this phase shift will be accumulated. For 200 days of duration, the accumulated phase shift reaches $\Delta\phi \approx -1.08 \times 10^{-11}$. This value is the same order of magnitude as that of a gravitational wave signal [21], and could be detected by current technologies developed for ground-based gravitational wave observatories [22].

The example given above is purely indicative and aims to show that a detectable phase shift could be produced by present-day technology. We can give a simple order of magnitude and lower bound of the accumulated phase shift

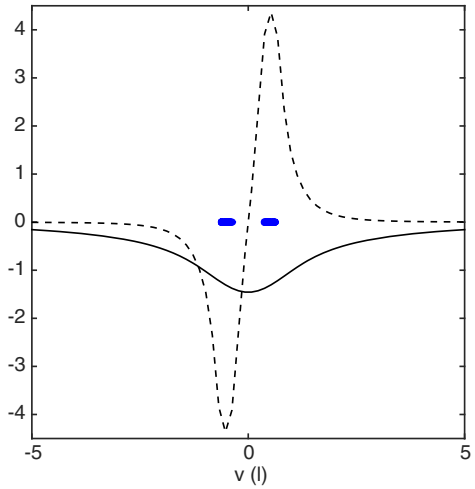

FIG. 8. $(\rho(0,v)-\lambda(0,v))/\mathcal{C}_I$ (straight line) and magnetic field $B_z(0,v)/(\mu_0 NI)$ (dashed line) along the axis of symmetry of the anti-Helmholtz coil ($\mu_0 NI = 4.4T$). Dots indicate the position of the solenoids along the z axis.

produced by posing $\rho-\lambda \approx \mathcal{C}_I$ on the axis of symmetry so that the phase shift Eq. (42) gives

$$\Delta\Phi \approx \pi\frac{\mathcal{L}}{\Lambda}\mathcal{C}_I \times \frac{T_{\text{exp}}}{t_{\text{bounce}}} \approx \pi\frac{\mathcal{C}_I}{\Lambda}cT_{\text{exp}} \tag{45}$$

where T_{exp} is the duration of the experiment and t_{bounce} is the time taken by light to produce a bounce inside the interferometer so that $T_{\text{exp}}/t_{\text{bounce}} = N_{\text{bounce}}$ is the number of bounces inside the Fabry-Pérot cavity.

To conclude this section, we emphasize that the generation and detection of artificial gravitational fields by strong magnetic fields is within experimental reach but requires large multilayered superconducting magnets powered during dozens of days as well as 100-m-long Michelson interferometers with Fabry-Pérot cavities that could achieve the same sensitivity as ground-based gravitational wave observatories but in the presence of intense magnetic fields. As in gravitational wave observatories, a long optical path is crucial for the detection of the very weak gravitational perturbations. However, the wave front of an astrophysical gravitational wave is much longer than the perturbations of spacetime generated by electromagnets a decameter large. Therefore, a kilometer-wide interferometer can fit into the gravitational wave front coming from astrophysical sources and is necessary to capture the wave during the time it passes through Earth. Using a kilometer-large interferometer for the detection of the spacetime curvature induced by superconducting coils would require kilometer-large magnets. This is not necessary since, unlike the detection of gravitational waves, spacetime deformation by electromagnets is maintained as long as the magnetic field is present. The amplitude of this spacetime deformation is extremely tiny, of order of $\mathcal{C}_I$, which requires us to trap the light long enough inside the spacetime deformation to accumulate enough phase shift for detection. Although experimentally challenging, such a detection would open the path to a new class of laboratory tests of general relativity and the equivalence principle.

VI. CONCLUSIONS

The generation of artificial gravitational fields with electric currents could be in principle detected through the induced change in spacetime geometry that results in a purely classical deflexion of light by magnetic fields. This effect does not invoke any new physics, as it is a consequence of the equivalence principle. Although very weak, we have shown that this effect could be detectable by a twofold experimental setup. On one hand, it includes stacked large superconducting Helmholtz coils for the generation of the artificial gravitational field. On the other hand, the detection would be achieved by highly sensitive Michelson interferometers whose arms contain Fabry-Pérot cavities to store light into the generated gravitational field. In an appropriate experimental setup, the amplitude of the phase shift accumulated during the bouncing of light in the curved spacetime generated by the magnetic field would reach in a few months the level of an astrophysical source of gravitational wave passing through ground-based gravitational wave observatories.

We claim that such detection would open new eras in experimental gravity and laboratory tests of general relativity and the equivalence principle. These tests, although concerning the weak field regime, will have the particularity of focusing exclusively on the coupling between gravitation and electromagnetism. Future theoretical works should focus on extending the present study to alternative theories of gravity to explore how far they would depart from general relativity.

Such a detection of the spacetime curvature generated by a magnetic field in the laboratory would constitute a major step in physics: the ability to produce, detect, and ultimately control artificial gravitational fields. And would this technology be developed, it could lead to amazing applications like the controlled emission of gravitational waves with large alternative electric currents. Gravity would then cease to be the last of the four fundamental forces not under control by human beings.

ACKNOWLEDGMENTS

The author is very grateful to M. Rinaldi and A. Hees for the fruitful discussions which significantly helped to extend the preliminary work and ended up with the results presented as an application. This research used resources of the "Plateforme Technologique de Calcul Intensif (PTCI)" (http://www.ptci.unamur.be) located at the University of Namur, Belgium, which is supported by the F.R.S.-FNRS under the convention Grant No. 2.4520.11. The PTCI is member of the "Consortium des Équipements de Calcul Intensif (CÉCI)" (http://www.ceci-hpc.be).

[1] Their strength differs by a factor of about 10^{-40} in a hydrogen atom.
[2] T. Levi-Cività, Gen. Relativ. Gravit. **43**, 2307 (2011); B. Bertotti, Phys. Rev. **116**, 1331 (1959); I. Robinson, Bull. Acad. Pol. Sci., Sér. sci. tech. **7**, 351 (1959).
[3] B. Mukherji, Calcutta Math. Soc. Bull. **30**, 95 (1938).
[4] L. Witten, Centre Belge de Recherches Mathématiques, Colloque sur la Théorie de Relativité, 1960, p. 59; in *Gravitation: An Introduction to Current Research*, edited by L. Witten (Wiley, New York, 1962), Chap. 9.
[5] W. B. Bonnor, Proc. Phys. Soc. London Sect. A **67**, 225 (1954).
[6] W. B. Bonnor, Proc. Phys. Soc. London Sect. A **76**, 891 (1960).
[7] B. V. Ivanov, Mod. Phys. Lett. A **09**, 1627 (1994).
[8] The relevant fundamental constants of the EM system are G as Newton's constant, c as the speed of light and μ_0 as the (vacuum) magnetic permeability.
[9] Experimentally, any effect of the mass carriers can easily be handled by calibrating the experiment in the absence of electric currents.
[10] H. Weyl, Ann. Phys. (Berlin) **359**, 117 (1917).
[11] J. D. Jackson, *Classical Electrodynamics* (Wiley, New York, 1998).
[12] L. Landau, E. Lifchitz, and L. P. Pitaevskii, *Electrodynamics of Continuous Media* (Pergamon, New York, 1984).
[13] E. E. Callaghan and S. H. Maslen, NASA Technical Note No. D-465, 1960.
[14] The magnetogravitational coupling $\mathcal{C}_I$ can also be rewritten:
$$\mathcal{C}_I = 8\pi\left(\frac{I}{I_{\mathrm{Pl}}}\right)^2,$$
where I represents the total current involved and $I_{\mathrm{Pl}} = c^2/\sqrt{G\mu_0} = 9.8169 \times 10^{24} A$ is the Planck current.
[15] L. F. Shampine, I. Gladwell, and S. Thompson, *Solving ODEs with MATLAB* (Cambridge University Press, Cambridge, England, 2003).
[16] This can be viewed by evaluating the classical Maxwell equation Eq. (8) with the numerical implementation of a_{nr}.
[17] S. Blatt *et al.*, Phys. Rev. Lett. **100**, 140801 (2008).
[18] B. Linet and P. Tourrenc, Can. J. Phys. **54**, 1129 (1976); L. Stodolsky, Gen. Relativ. Gravit. **11**, 391 (1979); P. Delva, M.-C. Angonin, and P. Tourrenc, Phys. Lett. A **357**, 249 (2006).
[19] *Experimental Physics of Gravitational Waves*, edited by M. Barone, G. Calamai, M. Mazzoni, R. Stanga, and F. Vetrano (Proceedings of the International Summer School, Urbino, Italy, 2000).
[20] G. Acquistapace, CERN/LHCC Report No. 97–10 CMS TDR 1, 1997.
[21] A gravitational wave coming from astrophysical sources, however, produces the same amplitude in time scales of a millisecond.
[22] B. S. Sathyaprakash and B. F. Shutz, Living Rev. Relativity **12**, 2 (2009).